The GCM Oriented Calipso Cloud Product (CALIPSO-GOCCP)

H. Chepfer[(1)], S. Bony[(1)], D. Winker[(2)], G. Cesana[(3)], JL. Dufresne[(1)], P. Minnis[(2)], C. J. Stubenrauch[(3)], S. Zeng [(4)]

[(1)] LMD/IPSL, Univ. Paris 06, CNRS, Paris, France.

[(2)] NASA/LaRC, Hampton, VA, USA.

[(3)] LMD/IPSL, CNRS, Ecole Polytechnique, Palaiseau, France.

[(4)] LOA, Univ. Lille, Lille, France

Submitted to J. Geophys. Res., Special Issue Calipso, 15 April 2009

Abstract. This paper presents the GCM-Oriented Cloud-Aerosol Lidar and Infrared Pathfinder Satellite Observations (CALIPSO) Cloud Product (CALIPSO-GOCCP) designed to evaluate the cloudiness simulated by General Circulation Models (GCMs). For this purpose, CALIOP L1 data are processed following the same steps as in a lidar simulator used to diagnose the model cloud cover that CALIPSO would observe from space if the satellite was flying above an atmosphere similar to that predicted by the GCM. Instantaneous profiles of the lidar Scattering Ratio (SR) are first computed at the highest horizontal resolution of the data but at the vertical resolution typical of current GCMs, and then cloud diagnostics are inferred from these profiles: vertical distribution of cloud fraction, horizontal distribution of low-mid-high and total cloud fractions, instantaneous SR profiles, and SR histograms as a function of height. Results are presented for different seasons (January-February-March 2007-2008 and June-July-September 2006-2007-2008), and their sensitivity to parameters of the lidar simulator is investigated. It is shown that the choice of the vertical resolution and of the SR threshold value used for cloud detection can modify the cloud fraction by up to 0.20, particularly in the shallow cumulus regions. The tropical marine low-level cloud fraction is larger during nighttime (by up to 0.15) than during day-time. The histograms of SR characterize the cloud types encountered in different regions.

The GOCCP high-level cloud amount is similar to that from TOVS, AIRS. The low-level and mid-level cloud fractions are larger than those derived from passive measurements (ISCCP, MODIS-CERES POLDER, TOVS, AIRS).

Introduction

The definition of clouds or cloud types is not unique. It differs among observations (e.g. clouds detected by a lidar may not be detected by a radar or by passive remote sensing), and between models and observations (e.g. models predict clouds at each atmospheric level where condensation occurs, while observations may not detect clouds overlapped by thick upper-level clouds). A comparison between modelled and observed clouds thus requires a consistent definition of clouds, taking into account the effects of viewing geometry, sensors' sensitivity and vertical overlap of cloud layers. For this purpose, clouds simulated by climate models are often compared to observations through a model-to-satellite approach: model outputs are used to diagnose some quantities that would be observed from space if satellites where flying above an atmosphere similar to that predicted by the model [e.g., *Yu et al.*, 1996, *Stubenrauch et al.* 1997, *Klein and Jacob*, 1999, *Webb et al.*, 2001, *Zhang et al.*, 2005, *Bodas-Salcedo et al.*, 2008, *Chepfer et al*,. 2008, *Marchand et al.*, 2009].

Within the framework of the Cloud Feedback Model Intercomparison Program (CFMIP, http://www.cfmip.net), a package named COSP ("CFMIP Observation Simulator Package") has been developed to compare in a consistent way the cloud cover predicted by climate models with that derived from different satellite observations. This package includes in particular an ISCCP (International Satellite Cloud Climatology Project) simulator [*Klein and Jacob*, 1999, *Webb et al.*, 2001], a CloudSat simulator [*Haynes et al.*, 2007], and a Cloud-Aerosol Lidar and Infrared Pathfinder Satellite Observations (CALIPSO) simulator [*Chepfer et al.*, 2008). Additionally, it includes a Subgrid Cloud Overlap Profile Sampler [*Klein and Jacob*, 1999] that divides each model grid box into an ensemble of sub-columns generated stochastically and, in which, the cloud fraction is assigned to be 0 or 1 at every model level, with the constraint that the cloud condensate and cloud fraction averaged over all sub-

columns is consistent with the grid-averaged model diagnostics and the cloud overlap assumption.

The purpose of this paper is to present a dataset (named CALIPSO-GOCCP) that diagnoses cloud properties from CALIPSO observations exactly in the same way as in the simulator (similar spatial resolution, same criteria used for cloud detection, same statistical cloud diagnostics). This ensures that discrepancies between model and observations reveal biases in the model's cloudiness rather than differences in the definition of clouds or of diagnostics.

Section 2 describes the processing of CALIPSO Cloud-Aerosol Lidar with Orthogonal Polarization (CALIOP) Level 1 data [*Winker et al*. 2007] leading to the GOCCP dataset, and presents globally-averaged results for June-July-August (JJA) 2006-2008 and January-February-March (JFM) 2007-2008. The sensitivity of observed cloud diagnostics to the vertical resolution and to the cloud detection threshold is evaluated in Section 3. Day/night variabilities of cloud characteristics are discussed in Section 4, together with an illustration of GOCCP results along the Global Energy and Water Cycle Experiment (GEWEX) Pacific Cross-section Intercomparison transect (GPCI, http://gcss-dime.giss.nasa.gov/gpci/modsim_gpci_models.html). GOCCP results are then compared with other cloud climatologies in Section 5, and conclusions are drawn in Section 6.

2. Processing of CALIOP Level 1 data

2a. Calculation of the Scattering Ratio

Here we use the ATtenuated Backscattered profile at 532nm (ATB, collection V2. 01) that is part of the CALIOP lidar Level 1 dataset. CALIOP is aboard the CALIPSO, a nearly sun-synchronous platform that crosses the equator at about 0130 LST [*Winker et al*. 2007, 2009].

The original ATB horizontal resolution is 330 m below and 1 km above 8 km of altitude, and the vertical resolution is 30 m below and 60 m above 8km, with a total of 583 vertical levels distributed from the surface up to 40 km. The Molecular Density profile (MD) is derived from Goddard Modeling and Assimilation Office (GMAO*)* atmospheric profiles [*Bey et al.* 2001] for 33 vertical levels.

In the COSP software, both the CALIPSO and the CloudSat simulator results are computed on a vertical grid of 40 equidistant levels (height interval, Δz = 480 m) distributed from the sea level to 19 km. The ATB profile (583 vertical levels, Fig. 1a) and the MD profile (33 vertical levels) are each independently averaged or interpolated onto the 40-level vertical grid, leading to the ATB_{vert} and MD_{vert} profiles. This averaging significantly increases the ATB signal-to-noise ratio.

To convert the MD profile into molecular ATB, ATB_{vert} and MD_{vert} profiles are analyzed and averaged in cloud-free portions of the stratosphere: $22 < z < 25$ km for night time data ($20 < z < 25$ km for day time), and $28.5 < z < 35$km in the Southern Hemisphere (60°s to 90°S) during winter (June to October) to avoid Polar Stratospheric Clouds. At these altitudes z, ATB_{vert} and MD_{vert} profiles are each averaged horizontally over +/-33 profiles (+/-10 km) on both sides of a given profile.

The ratio between these two values ($R = \langle ATB_{vert} \rangle / \langle MD_{vert} \rangle$) is then applied to the entire initial instantaneous profile ATB_{vert} (not averaged horizontally) to convert the MD_{vert} profile into an ATtenuated Backscatter Molecular signal profile ($ATB_{vert,mol}$). This latter represents the ATB profile that would be measured in the absence of clouds and aerosols in the atmosphere. The lidar scattering ratio (SR) vertical profile is then computed by dividing the ATB_{vert} profile by the $ATB_{vert,mol}$ profile. Its horizontal resolution is 330 m and the vertical resolution is close to that of GCMs (Figures 1b,d and 2b,d)

Despite the vertical averaging, the signal-to-noise ratio remains low during daytime in clear-sky regions because of the large number of solar photons reaching the lidar's telescope

(Figures 2b and d). Daytime profiles with R values significantly different from those taken at nighttime ($R > 0.95$ or $R < 0.14$) are rejected. They represent about 30% of the total number of Level 1 V2.01 daytime profiles (e.g., Figure 2c). Pixels located below and at the surface level are rejected by using the 'altitude-elevation' flag from level 1 CALIOP data.

2b. Definition of cloud diagnostics

Vertical Profile of the cloud fraction

Several simple diagnostics are derived from the SR profile. Different SR thresholds are used to label each atmospheric layer (Figures 1d and 2d) as *cloudy* (SR > 5), *clear* (0.01 < SR < 1.2), *fully attenuated* (SR < 0.01), or *unclassified* (1.2 < SR < 5 or ATB-ATB_{mol} < $2.5.10^{-3}$ $km^{-1}.sr^{-1}$) to avoid false cloud detection in the upper troposphere / lower stratosphere, where the ATB_{mol} is very low. We then derive the *low-level* (P > 680 hPa), *middle-level* (440 < P < 680 hPa), *high-level* (P < 440 hPa) and total cloud fractions. To keep detailed information about the distribution of the signal intensity, we also consider the *histograms of SR values* (referred as SR CFAD532 in the GOCCP dataset*)* that summarize the occurrence frequency of different SR values (we use 15 intervals of SR values, ranging from 0 to 100) as a function of height (y-axis).

Maps

Monthly cloud fractions are then computed at each vertical level (or at low-, middle-, and upper-level layers) by dividing, for each longitude-latitude grid box, the number of cloudy profiles encountered during one month by the total number of instantaneous SR profiles (not fully attenuated) measured during that month. In the GOCCP database, cloud-layer diagnostics are referred to as "*Maps of Low – Mid – High clouds"* and monthly mean three-dimensional distributions of the cloud fraction as *"3D Cloud Faction"*.

Monthly SR histograms (which provide information about the variability of the SR signal) are also computed by accumulating the instantaneous SR histograms over a month in each grid box and each vertical layer. Each of these diagnostics has its counterpart included in the lidar simulator outputs of COSP.

2.c. June-July-August and January-February-March results

In this section we present the seasonal mean results for JJA and JFM obtained for the 40 levels vertical grid and for a horizontal resolution of 2.5° (latitude) x 3.75° (longitude).

(i) Maps of total and layered cloud fractions.

As shown by Table 1, the globally averaged total cloud cover is 0.66, and is greater over ocean (0.71) than over land (0.57). As expected, Figure 3a shows that the minimum total cloud cover occurs over sub-tropical deserts (Sahara, South Africa, Australia, etc), and the maxima are found over the Inter-Tropical Convergence Zone (ITCZ), the mid-latitudes storm tracks, and the eastern sides of the ocean basins associated with persistent low-level stratiform cloudiness. Maps of low-level, mid-level and upper-level cloud types (Figures 3b-d) show the predominance of low-level clouds over the oceans, both in the tropics and in the extra-tropics, and a striking land-sea constrast in the low-level cloud fraction. Low-level cloud fractions of about 0.3-0.4 are found in the trade wind areas (typically covered by shallow cumulus clouds), while amounts exceeding 0.6 occur in the mid-latitudes. Small low-level cloud fractions are reported only in the deep convective regions (warm pools, ITCZ), where thick upper-level clouds attenuate the lidar signal so much that low-level clouds cannot be detected. Overall. the change in total cloud amount is less than 0.01 between JJA and JFM (Table 1). The main seasonal cloud fraction variation (Figures 3e-h for JJA vs. Figures 3a-d for JFM) occurs in tropical regions (between 30°N and 20°S), where both oceanic and land cloud cover

changes follow the seasonal latitudinal migration of the ITCZ. The mid and high cloud cover seasonal variations are similar (Figure 3) because the mid-level clouds are typically associated with high clouds. The largest seasonal variation for both cloud layers is associated with deep convection over continents.

(ii) Vertical distribution of clouds.

The zonally averaged vertical distribution of the GOCCP cloud fraction, together with the fractional area of each grid box (or each latitude) associated with clear-sky or undefined situations, are shown in Figure 4. At each altitude, the sum of cloudy, clear, undefined areas is equal to 1. The zonal mean cloud fraction is maximal within the atmospheric boundary layer (below 3 km), except at very low latitudes where upper-level clouds mask lower-level clouds (as indicated by the maximum of the fully attenuated fraction). The mid-latitude cloudiness occurs at all levels of the atmosphere, with a maximum at low levels. Such a structure is expected in regions where baroclinic instabilities produce frontal clouds over the whole depth of the troposphere and where anticyclonic situations produce boundary-layer clouds. Equatorward of about 10° of latitude, the cloud fraction is greatest at heights between 12 and 14 km. In the Tropics, this atmospheric layer where extensive anvil clouds are formed by the detrainment of hydrometeors from convective systems [e.g. *Folkins et al*., 2000].

The uncertain situations (Figure 4d) correspond to cases in which the SR signal is too high for a clear-sky situation, but is too low to unambiguously define the presence of a cloud layer. These situations may occur where boundary-layer aerosols are abundant (e.g. over the Atlantic windward of the Sahara), or where the cloudiness is to thin or too broken to pass the cloud detection threshold (SR=5).

(iii) SR histograms

Histograms of SR provide a summary of the occurrence of the different SR values encountered within a gridbox at a given altitude. Each histogram is normalized by dividing the occurrence in each SR-altitude box by the total number of occurrences in the histogram. This diagnostic is the lidar counterpart of the joint height-reflectivity histogram derived from Cloudsat radar data for comparable vertical grids [e.g. *Zhang et al.*, 2007, *Bodas et al*., 2008, *Marchand et al*., 2009].

Figure 5 shows histograms of SR aggregated for various regions and for two seasons (JFM and JJA). Those exhibit different patterns depending on the prominent cloud types in presence. Over the Tropical Western Pacific warm pool, deep convective cloud systems produce many large SR values (> 10) at altitudes between 12 and 15 km (Fig. 5a) and numerous cases of fully attenuated values (SR < 0.01) below 8 km (related to the attenuation of the low-altitude lidar signal by the overlapping thick cloud layers). Secondary maxima in the SR histogram also appear in the mid-troposphere (5 - 9 km), which is consistent with the large abundance of thick congestus clouds over this region [*Johnson et al.*, 1999], and at low-levels (below 3 km) associated with the presence of small shallow cumulus clouds. On the contrary, the SR histogram associated with California stratocumulus clouds exhibits two distinctive maxima: the first one below 3 km, where numerous low-level clouds produce a wide range of SR values between 3 and 80, and the second one around 10 km associated with the presence of thin cirrus clouds. Note that values of $3 < SR < 5$ above 14 km are due to observational noise and thus have no geophysical meaning; they do not pass the test, $ATB - ATB_{mol} < 2.5.10^{-3}$ $km^{-1}.sr^{-1}$ (defined in Sect. 2b). In the mid-latitude North Pacific region, the SR histogram exhibits a large range of SR values over the whole troposphere and a substantial number of fully attenuated values below 5 km, consistent with the presence of thick, high-topped frontal clouds of large vertical extent in regimes of synoptic ascent (e.g. baroclinic fronts) and the presence of low-level clouds in regimes of synoptic descent [e.g., *Lau and Crane*, 1995; *Norris and Iacobellis*, 2005].

3. **Sensitivity to horizontal and vertical averaging, and to cloud detection thresholds.**

(i) Sensitivity to horizontal sampling

All the GOCCP cloud diagnostics are derived at the full horizontal resolution of CALIOP Level 1 data (330 m along the track below 8 km and 1 km above 8 km). They are based on a procedure that, at this resolution, declares each atmospheric layer as totally "clear", "undefined", "fully attenuated" or "cloudy" (to be consistent with the lidar simulator). Because, as in nature, clouds exhibit a very wide range of sizes the cloud detection is sensitive to the horizontal resolution of the data. As a test of this sensitivity, we examined the impact of resolution on the diagnosed cloud fraction by horizontally averaging the lidar signal over each10 km prior to cloud detection. The results (not shown) indicate that the horizontal averaging can induce an artificial overestimate of the observed cloud cover in broken low cloud cumulus fields. The overestimate ranges up to about 20 to 25% in the trade cumulus regime. This can be understood by considering the following idealized example: a single low-level liquid water cloud of small size (e.g., 1-km radius) surrounded by clear-sky can produce locally a strong lidar backscattered signal (and thus a high SR value) which, once averaged with the surrounding clear sky profiles, can lead to an SR value passing the cloud detection threshold (SR=5). In such a case, a pixel of 10-km in length may thus be declared as overcast although the actual cloudiness covers only one hundredth of the area of that pixel.

The GOCCP cloud detection is thus made at the full resolution of the original CALIOP level 1 data to ensure that the cloud cover is not artificially overestimated in regions where clouds have typical sizes larger than or on the order of this resolution (75 m cross-track and 330 m along track below 8 km).

(ii) Sensitivity to the vertical grid resolution

A pre-requisite for a consistent model-data comparison of the cloud fraction is that cloud layers are defined similarly in observations and in model outputs. Using lidar signals to diagnose cloud layers requires that similar SR thresholds are used for cloud detection and that these thresholds are applied at the same vertical resolution. COSP diagnostics from climate models may be analyzed either at the vertical resolution of each models (which varies from one model to another), or over a pre-defined vertical grid of 40 equidistant levels (the so-called "COSP grid"). Here, we examine the impact of vertical resolution on GOCCP cloud diagnostics.

The initial CALIOP L1 data contains 583 levels having 30-m spacing between the surface and 8 km and 60-m spacing above 8 km. As shown in Figure 1, averaging CALIOP L1 data over the 40-level grid significantly increases the signal-to-noise ratio, and therefore minimizes the risk of false cloud detections. *Chepfer et al.* [2008] derived the CALIPSO cloud fraction for a coarser vertical grid, corresponding to the 19 vertical levels of the standard version of the LMDZ4 GCM, with 6 levels at low altitudes (*below 3 km*), 3 levels at middle heights (*between 3 and 7.2 km*), and 10 levels in the upper troposphere (*above 7.2 km*). In the 40-level grid, the "low-level", "mid-level" and "upper-level" atmospheric layers are comprised of 7, 8 and 25 levels, respectively.

The total cloud cover obtained for 19 levels is about 0.05 lower than for 40 levels (Table 1 and 2), but this discrepancy is much more significant for the upper-level cloud fraction (up to 0.20 difference over tropical continents in the Southern Hemisphere). Vertical averaging lessens the contribution of optically thin cirrus clouds to the SR signal and, therefore, decreases the probability of passing the cloud detection threshold (Figure 1d). Thus, reducing the vertical resolution decreases the high-level cloud amount and, more generally, the cloud fraction associated with thin stratiform cloud layers. Figure 6 shows

that this effect also impacts low and mid level cloud amounts with larger differences (up to 0.05) at latitudes poleward of 60°.

(iii) Sensitivity to the cloud detection threshold

The cloudy threshold value (here SR=5) is a parameter of the lidar simulator that affects the detection of the optically thinner clouds. The higher the SR threshold is, the lower the cloud fraction will be and the more optically thin clouds will be missed. Typically, assuming a homogeneous boundary layer water cloud with a geometrical thickness of 250 to 500 m and a liquid particle radius of 12 μm, a value SR=5 corresponds to an optical depth of 0.03 - 0.05 and an LWP of 0.1 - 0.2 g/m^2. Based on this estimate, most semi-transparent clouds (optical depth > 0.03) are detected, but most subvisible ones are missed. On the other hand, some dense dust layer can be classified as cloudy when applying a simple cloud detection threshold based on SR alone. To test the sensitivity of our results to this threshold value, we computed cloud fractions for a threshold value of 3, which would detect clouds having an optical depth larger than about 0.015.

When the cloud detection threshold is reduced, the mean total cloud fractions increase by about 0.05 during night time and by up to 0.10 during daytime (Table 3). Figure 7 shows that the total cloud cover is shifted to greater values at all latitudes except over polar regions. High-level clouds (not shown) do not contribute significantly to this increase. Sub-visible clouds, that may occur, for instance, above the overshoot regions [*Dessler*, 2005], are missed by both thresholds (SR=3 and SR=5). The total cloud cover increase is primarily driven by the global increase of the tropical low-level cloud fraction (Table 3 and Fig. 7c). This latter results from a more frequent detection of optically thin and/or broken boundary layer clouds, most likely to be shallow cumulus. The mid-level cloud fraction also increases in the Tropics in the area of large deserts (Figure 7b) when decreasing the cloud detection threshold, especially for daily observations (Table 3). It may be that the SR=3 threshold detects some

large smoke or dust loading events occurring in summer, and/or to the presence of thin clouds at the top of the Saharan atmospheric boundary layer.

4. Day-night and regional cloud variations.

(i) Day-night differences

The clear-sky daytime CALIOP data are much noisier than those at night (Figure 1 vs. Figure 2) because of the solar photons, About 30% of the daytime profiles are rejected after quality test on the normalization of CALIOP Level 1 V2 data (Sect. 2a). We examine the day-night cloud cover differences to check whether the daytime data introduce a bias in the mean day/night results. The total day-night cloud cover difference is small at the global scale (< 0.01, Table 1). The largest differences occur over continents where clouds are slightly more frequent during daytime at all altitudes (Table 1), but the day-night variation depends on the vertical resolution (Table 2 for the coarse grid vs. Table 1 for CFMIP) and on the cloudy threshold value (SR=3 or SR=5, Table 3).

Maps of day-night differences (Figure 8a) show that clouds are more frequent over continents during daytime (13:30 local time), whereas low-level clouds are more frequent (15%) during night-time (1:30 local time) than during daytime in the tropical subsidence regions. Examination of the low, mid, high cloud amounts independently reveals that the total day-night cloud cover variation is mostly driven by low level clouds (Figure 8b). Both the geographical patterns and the order of magnitude of the day-night differences are in agreement with the High Resolution Infrared Sounder (HIRS) observations reported by *Wylie* [2008)]. This suggests that the day-night variation found in GOCCP is not an artefact of the noise associated with solar photons, but corresponds to the actual diurnal variation of clouds.

(ii) A regional scale example: along the GPCI transect

To evaluate the cloudiness simulated by weather and climate models, the GEWEX Cloud System Study has defined a transect, named the GEWEX Pacific Cross-section Intercomparison (GPCI, http://www.igidl.ul.pt/cgul/projects/gpci.htm) transect (black line on Figure 3a), that samples the stratocumulus region off the coast of California (35°N), the trade winds associated with shallow cumulus clouds, and the deep convective regions of the ITCZ (0-12°N). The mean JJA cloud fractions along this transect are shown in Figure 9a. The stratocumulus and shallow cumulus remain below altitudes of 2400 m with most below 2000 m, and their top heights increase from 1 to 2 km away from the coast. Deep convective clouds are mostly located below 17 km, and the lidar signal is fully attenuated below 8 km (not shown), meaning that the mean cloud optical depth between 8 and 17 km is typically on the order of 3. (The optical depth of the total column can be much larger than that.) The low-level cloud fraction exceeds 0.70 (Figure 9b) along the coast and decreases southward where the mid and high cloud cover increases, masking some of the low clouds. The diagram of SR along the transect (not shown) exhibits two maxima at low altitudes: high values of SR (> 60) associated with stratocumulus clouds and low values (SR<20) corresponding to cumulus clouds.

5. Comparison with other cloud climatologies

The availability of satellite measurements for more than 25 years has led to several global climatologies of cloud properties. They are being intercompared within the framework of the GEWEX cloud assessment (http://climserv.ipsl.polytechnique.fr/gewexca). The International Satellite Cloud Climatology Project (ISCCP, *Rossow and Schiffer* [1999]) has been deriving

cloud properties since 1983 using data taken by geostationary and polar orbiting weather satellites. Average ISCCP cloud amounts were computed for the period from 1984 to 2004, using 3-hourly daytime measurements from one infrared (IR) and one visible atmospheric window channel at a spatial resolution of about 7 km, sampled every 30 km. Due to their relatively good spectral resolution, IR sounders, like the HIRS of the TIROS-N Operational Vertical Sounder (TOVS) system aboard the National Oceanic and Atmospheric Administration (NOAA) satellites or the Atmospheric InfraRed Sounder (AIRS) aboard the Earth Observing Satellite (EOS) satellite Aqua, provide reliable cirrus detection during day and night. These data have been analyzed by *Stubenrauch et al.* [2006, 2008] to produce alternate long-term cloud climatologies. A shorter term climatology of clouds is being derived from low-Earth orbiting satellites by the Clouds and the earth's Radiant Energy System (CERES) project, which began in 1998 with the Tropical Rainfall Measuring Mission satellite, is currently operating aboard the EOS Aqua and Terra satellites, and will continue on other satellites in the future. The Aqua CERES cloud amounts and heights reported here were determined from MODerate-resolution Imaging Spectroradiometer (MODIS) data for the period July 2002- July 2007 using the methods of *Minnis et al.* [2008, 2009] and *Trepte et al.* [2002]. The results are denoted as CERES-MODIS data. The PARASOL cloud products for the period January 2006 – December 2008 are derived during daytime from multispectral (visible and near infrared only) and multiangle measurements from the Polarisation and Directionality of the Earth Reflectances (POLDER) instrument at a native resolution of 6 km x 6 km [*Parol et al.*, 2004].

Figure 10 presents the annually-averaged global cloud cover, separately for ocean and land areas, as obtained from CALIPSO GOCCP, ISCCP, AIRS-LMD, TOVS Path-B, CERES-MODIS and POLDER3/PARASOL. For a more consistent comparison between these cloud climatologies derived from passive remote sensing and GOCCP, a version of CALIPSO GOCCP (referred to as CALIPSO-GOCCP-5-no-overlap) has been treated in such a way that

only the highest cloud layer is taken into account. All averages are area weighted. The total cloud cover varies from 58% to 76%, depending on the sensitivity of the instrument or the retrieval algorithm or the handling of partly cloudy footprints. All climatologies show ~10 percent more cloud cover over ocean than over land, with more low-clouds over ocean than over land and about the same amount of high clouds over ocean and land. The cloud cover of AIRS-LMD is less than that from TOVS Path-B and slightly lower than that from ISCCP, because it corresponds to clouds for which cloud properties can be reliably determined [*Stubenrauch et al.*, 2008]: a weighted χ^2 method provides cloud pressure and cloud emissivity for about 90% of all AIRS footprints (13 km at nadir). When adding the eliminated partly cloudy footprints, weighted by a factor of 0.3, the cloud fraction rises from 0.63 to 0.71, indicating the uncertainty of cloud cover due to partly cloudy footprints. CALIOP appears to be the instrument most sensitive to cirrus, providing a high cloud cover of about 32% for CALIOP-GOCCP-5 and 40% for CALIOP-NASA (Winker et al. 2008), while the IR sounders provide about 30%, ISCCP about 22.5%, MODIS-CERES 20% and PARASOL only about 10%. POLDER high cloud amount is much less than all other climatologies due to (i) its limited ability to detect thin high clouds (no IR channels available), (ii) because O_2 cloud apparent pressure is only derived over land for optical thicknesses greater than 2.0 and (iii) because O_2-derived cloud apparent pressure tends to correspond to the middle of cloud pressure level [*Vanbauce et al.*, 2003]. Cirrus above low clouds are often misidentified as mid-level clouds by ISCCP [e.g. *Stubenrauch et al*., 1999] as well as by POLDER and CERES-MODIS. This may explain why the mid-level cloud fraction from ISCCP is larger than that of other climatologies obtained from passive remote sensing and that obtained from Calipso when identifying only the uppermost cloud layer (CALIPSO-GOCCP-5-no-overlap).

The mid-level and low-level cloud fractions from CALIPSO-GOCCP-5 are larger than that derived from ISCCP, because in addition to the uppermost cloud layers also those are taken into account which are underneath higher clouds (therefore the sum of all cloud type

fraction is larger than the total cloud fraction). The comparison of CALIPSO-GOCCP-5 with CALIPSO-GOCCP-5-no-overlap shows that only about half of all low and mid-level clouds are single layer clouds. As a consequence, low-level cloud fractions observed with AIRS, CERES-MODIS, ISCCP and TOVS-B fall between CALIPSO-GOCCP-SR5 and CALIPSO-GOCCP-SR5-no-overlap (Figure 10)

6. Conclusion

A GCM-Oriented CALIPSO Cloud Product (GOCCP) has been developed from the CALIOP L1 dataset to make consistent comparisons between CALIOP observations and "GCM+lidar simulator" outputs. For this purpose, the full-horizontal-resolution CALIOP level 1 data were vertically averaged at a resolution comparable to that of GCMs (40 levels), and then simple thresholds were applied to SR profiles to classify each atmospheric layer as cloudy, clear, fully attenuated or unclassified. Maps of the total cloud fraction and of the low-mid-high layered cloud fractions, 3D vertical distributions of the cloud fraction and joint height-SR histograms were then analyzed. The sensitivities of the results to the vertical grid and to the value of the SR threshold used for cloud detection were also studied. When decreasing the cloudy SR threshold value, the cloud fraction increases because the optically thinnest layers are better detected, independent of altitude and surface type. The effect of changing the vertical resolution (from 40 equidistant levels to 19 sigma equidistant ones) is critical for all cloud categories.

The total and zonal mean cloud covers have been presented for two different seasons, JFM (January-February-March) and JJA (June-July-August) in accumulating 3 years of CALIOP observations (June 2006 to August 2008). The results show that large cloud fractions (> 40%) are located in the marine boundary layer and that they have a significant seasonal variability;

the contribution of the Southern hemisphere tropical oceans is very significant. The seasonal variation of the global cloud cover is weak (less than 0.01), as is the globally-averaged day-night variation. On average, the cloud cover is greater over ocean than over land. Despite the enhanced noise of the lidar profiles in clear sky during daytime (resulting in the rejection of about 30% of the daytime profiles in this study), the day-night cloud cover difference seems robust and shows similar patterns and amplitude as the ones reported in the literature: more low-level clouds during night time in the oceanic subsidence regions and more clouds during daytime over land. Marine low-level clouds exhibit two categories, associated with different ranges of SR values: optically thick clouds (SR > 60) and optically thin clouds (SR < 20). Selected regions (tropical Western Pacific, mid-latitude North Pacific, Hawaii trade cumulus and California stratocumulus) exhibit different types of SR histograms, showing the potential of such diagrams for characterizing the prominent cloud types encountered in these regions.

As recommended by the WCRP Working Group for Coupled Models (http://eprints.soton.ac.uk/65383), the COSP simulator (version v1.0) developed by CFMIP (to be made available on http://www.cfmip.net) is to be used by the climate modeling groups in some of the CMIP5 simulations [*Taylor et al.*, 2009] that will be assessed by the Fifth Assessment Report (AR5) of the Intergovernmental Panel on Climate Change (IPCC). The CALIPSO-GOCCP products presented in this paper are fully consistent with the outputs from the lidar simulator used in COSP v1.0, and they will be made available on-line through the GOCCP website (http://climserv.polytechnique.fr/cfmip-atrain). In the future, these data may thus be directly compared with the lidar simulator outputs from the CMIP5 simulations, and then be used to evaluate the cloudiness predicted by the different GCMs participating in CMIP5.

Acknowledgments.

The authors would like to thank NASA, CNES, Icare and Climserv for giving access to the CALIOP data. This work was financially supported by CNES and by ENSEMBLES. The AIRS-LMD data have been analyzed by Sylvain Cros. Thanks are due to Yan Chen and Sunny Sun-Mack (SSAI) for the CERES-MODIS data processing and to J. Riedi (LOA) for discussion and comments about POLDER3/PARASOL data.

References

Bodas-Salcedo A., M. J. Web, M. E. Brook, M. A. Ringer, S. F. Milton, and D. R. Wilson, 2008: Evaluation of cloud systems in the Met Office global forecast model using CloudSat data, *J. Geophys. Res*., 113, D00A13, doi:10.1029/2007JD009620.

Bony S. and J-L. Dufresne, 2005; Marine boundary layer clouds at the heart of tropical cloud feedback uncertainties in climate models, *Geophys. Res. Lett*., 32, No. 20, L20806, doi:10.1029/2005GL023851.

Bey, I., D. J. Jacob, R. M. Yantosca, J. A. Logan, B. D. Field, A. M. Fiore, Q. Li, H. Y. Liu, L. J. Mickley, M. G. Schultz, Global modeling of tropospheric chemistry with assimilated meteorology: Model description and evaluation*, J. Geophys. Res*., 106(D19), 23073-23096, 10.1029/2001JD000807, 2001.

Chepfer, H., S. Bony, D. M. Winker, M. Chiriaco, J.-L. Dufresne, and G. Seze (2008), Use of CALIPSO lidar observations to evaluate the cloudiness simulated by a climate model, Geophys. Res. Lett., 35, L15704, doi:10.1029/2008GL034207.

Dessler A. E., S. P. Palm, W. D. Hart, J. D. Spinhirne (2006), Tropopause-level thin cirrus coverage revealed by ICESat/Geoscience Laser Altimeter System, *J. Geophys. Res*., 111, D08203, doi:10.1029/2005JD006586.

Dessler A. E., S. P. Palm, J. D. Spinhirne (2006), Tropical cloud-top height distributions revealed by the Ice, Cloud, and Land Elevation Satellite (ICESat)/Geoscience Laser Altimeter System (GLAS), *J. Geophys. Res*., 111, D12215, doi:10.1029/2005JD006705.

Folkins, I., S. Oltmans, and A. Thompson (2000), Tropical Convective Outflow and Near Surface Equivalent Potential Temperatures, Geophys. Res. Lett., 27(16), 2549-2552.

Haynes, J. M., R. T. Marchand, Z. Luo, A. Bodas-Salcedo, and G. L. Stephens (2007), A multipurpose radar simulation package: QuickBeam, Bull. Am. Meteorol. Soc., 88(11), 1723–1727, doi:10.1175/BAMS-88-11-1723

Johnson, R. H, T. M. Rickenback, S. A. Rutledge, P. E. Ciesielski, and W. H. Schubert, 1999: Trimodal characteristics of tropical convection. *J. Climate*, 12, 2397-2418.

Klein S. A. and C. Jakob, 1999: Validation and sensitivities of frontal clouds simulated by the ECMWF model. *Mon. Wea. Rev*., 127, 2514-2531.

Lau, N. C and M. W. Crane, 1995: A satellite view of the synoptic-scale organization of cloud properties in midlatitude and tropical circulation systems. *Mon. Wea. Rev.*, 123, 1984-2006.

Marchand, R., J. Haynes, G. G. Mace, T. Ackerman, and G. Stephens (2009), A comparison of simulated cloud radar output from the multiscale modeling framework global climate model with CloudSat cloud radar observations, J. Geophys. Res., 114, D00A20, doi:10.1029/2008JD009790.

Minnis, P., et al. (2008), Cloud detection in non-polar regions for CERES using TRMM VIRS and Terra and Aqua MODIS data, *IEEE Trans. Geosci. Remote Sens.*, *46*, 3857-3884.

Minnis, P., et al. (2009), Cloud property retrievals for CERES using TRMM VIRS and Terra and Aqua MODIS data, *IEEE Trans. Geosci. Remote Sens.*, *submitted*.

Norris, J. R., and S. F. Iacobellis, 2005: North Pacific cloud feedbacks inferred from synoptic-scale dynamic and thermodynamic relationships. *J. Climate*, 18, 4862-4878.

Parol F., J.C. Buriez, C. Vanbauce, J. Riedi, L. C.-Labonnote, M. Doutriaux-Boucher, M. Vesperini, G. Sèze, P. Couvert, M. Viollier, F.M. Bréon (2004), Capabilities of multi-angle polarization cloud measurements from satellite: POLDER results., *Adv. Space Res.* , 33, 1080-1088

Rossow, W. B. and R. A. Schiffer (1999): Advances in understanding clouds from ISCCP, *Bull. Amer. Meteor. Soc*., 80, 2261-2287.

Stubenrauch, C. J., A. D. Del Genio, and W. B. Rossow (1997), Implementation of Sub-Grid Cloud Vertical Structure inside a GCM and its Effect on the Radiation Budget, *J. Climate*, 10, 273-287

Stubenrauch, C. J., W. B. Rossow, N. A. Scott, and A. Chédin, (1999), Clouds as seen by Infrared Sounders (3I) and Imagers (ISCCP): Part III) Spatial Heterogeneity and Radiative Effects. *J. Climate*, **12**, 3419-3442.

Stubenrauch, C. J., A. Chédin, G. Rädel, N. A. Scott, and S. Serrar, (2006), Cloud properties and their seasonal and diurnal variability from TOVS Path-B, *J. Climate*, *19*, 5531-5553.

Stubenrauch C., S. Cros, N. Lamquin, R. Armante, A. Chedin, C. Crevoisier, and N. A. Scott, (2008): Cloud properties from atmospheric infrared sounder and evaluation with cloud-aerosol lidar and infrared pathfinder satellite observations. *J. Geophys. Res*., 113, D00A10, doi:10.1029/2008JD009928.

Taylor, K. E., R. J. Stouffer, and G. A. Meehl, 2009 : A summary of the CMIP5 Experiment Design (http://www.clivar.org/organization/wgcm/references/Taylor_CMIP5_dec31.pdf).

Trepte, Q., P. Minnis, and R. F. Arduini (2002), Daytime and nighttime polar cloud and snow identification using MODIS data, *Proc. SPIE 3rd Intl. Asia-Pacific Environ. Remote Sensing Symp. 2002: Remote Sens. of Atmosphere, Ocean, Environment, and Space*, Hangzhou, China, October 23-27, *Vol. 4891*, 449-459.

Vanbauce C., B. Cadet, R. T. Marchand, (2003) Comparison of POLDER apparent and corrected oxygen pressure to ARM/MMCR cloud boundary pressures, *Geophys. Res. Letters* , 30-5, 16.1 – 16.4, doi:10.1029/2002GL016449

Webb M, C Senior, S Bony and J-J Morcrette, 2001: Combining ERBE and ISCCP data to assess clouds in three climate models, *Climate Dynamics*, 17, 905-922.

Winker D., W. Hunt, and M. McGill, 2007: Initial Performance Assessment of CALIOP, *Geophys. Res. Lett*., 34, L19803, doi:10.1029/2007GL030135.

Winker D., B. Getzewitch, and M. Vaughan, 2008: Evaluation and applications of Cloud Climatologies from CALIOP*, ILRC conf. REF?*

Winker D., M. A. Vaughan, A. Omar, Y. Hu, K. A. Powell, Z. Liu, W. H. Hunt, and S. A. Young, 2009: Overview of the CALIPSO mission and CALIOP data processing algorithms, J. Atmos. Ocean. Tech, in press

Wylie D. (2008): Diurnal cycles of clouds and how they affect polar-orbiting satellite data, *J. Clim*. 21, 3989-3996.

Zhang M H, W Y Lin, S A Klein, J T Bacmeister, S Bony, R T Cederwall, A D Del Genio, J J Hack, N G Loeb, U Lohmann, P Minnis, I Musat, R Pincus, P Stier, M J Suarez, M J Webb, J B Wu, S C Xie, M -S Yao and J H Zhang, 2005: Comparing Clouds And Their Seasonal Variations in 10 Atmospheric General Circulation Models With Satellite Measurements. *J. Geophys. Res*., 110, D15S02, doi:10.1029/2004JD005021.

Table 1: Cloud fraction from standard GOCCP (detection threshold SR=5 and COSP vertical grid of 40 equidistant vertical levels) for two seasons (JFM=January-February-March and JJA=June-July-August).

GOCCP		**JFM Night**	**JJA Night**	**JFM Day**	**JJA Day**
Global	**Total**	**0.66**	**0.66**	**0.66**	**0.66**
	Low	0.36	0.36	0.36	0.37
	Mid	0.20	0.19	0.27	0.25
	High	0.29	0.29	0.35	0.33
Land	**Total**	**0.55**	**0.54**	**0.61**	**0.61**
	Low	0.20	0.15	0.26	0.25
	Mid	0.26	0.24	0.32	0.31
	High	0.28	0.31	0.34	0.34
Ocean	**Total**	**0.71**	**0.71**	**0.68**	**0.68**
	Low	0.44	0.45	0.41	0.42
	Mid	0.18	0.17	0.24	0.23
	High	0.29	0.28	0.35	0.33

Table 2: Sensitivity to the vertical grid – cloud fraction diagnosed as in GOCCP but using a coarse vertical grid (19 vertical levels) instead of 40 levels.

Coarse GRID		**JFM Night**	**JJA Night**	**JFM Day**	**JJA Day**
Global	**Total**	**0.62**	**0.62**	**0.59**	**0.60**
	Low	0.34	0.34	0.35	0.36
	Mid	0.21	0.21	0.19	0.19
	High	0.16	0.16	0.16	0.16
Land	**Total**	**0.48**	**0.46**	**0.47**	**0.49**
	Low	0.16	0.12	0.20	0.19
	Mid	0.24	0.25	0.22	0.23
	High	0.15	0.17	0.13	0.14
Ocean	**Total**	**0.68**	**0.68**	**0.64**	**0.65**
	Low	0.42	0.44	0.42	0.43
	Mid	0.20	0.19	0.17	0.17
	High	0.16	0.16	0.16	0.16

Table 3: Sensitivity to the detection threshold – Cloud fraction diagnosed as in GOCCP but using a threshold value SR=3 instead of SR=5 for cloud detection.

JJA / Night		**GOCCP** SR3	**GOCCP** SR5	**GOCCP** Coarse Grid SR3	**GOCCP** Coarse Grid SR5
Global	**Total**	**0.70**	**0.66**	**0.68**	**0.62**
	Low	0.41	0.36	0.41	0.34
	Mid	0.21	0.19	0.22	0.21
	High	0.29	0.29	0.16	0.16
Land	**Total**	**0.57**	**0.54**	**0.49**	**0.46**
	Low	0.18	0.15	0.14	0.12
	Mid	0.27	0.24	0.26	0.25
	High	0.31	0.31	0.17	0.17
Ocean	**Total**	**0.76**	**0.71**	**0.76**	**0.68**
	Low	0.51	0.45	0.53	0.44
	Mid	0.18	0.17	0.20	0.19
	High	0.28	0.28	0.16	0.16

JJA / Day		**GOCCP** SR3	**GOCCP** SR5	**GOCCP** Coarse Grid SR3	**GOCCP** Coarse Grid SR5
Global	**Total**	**0,74**	**0.66**	**0,68**	**0.60**
	Low	0,46	0.37	0,46	0.36
	Mid	0,33	0.25	0,21	0.19
	High	0,34	0.33	0,16	0.16
Land	**Total**	**0,69**	**0.61**	**0,53**	**0.49**
	Low	0,33	0.25	0,24	0.19
	Mid	0,40	0.31	0,26	0.23
	High	0,35	0.34	0,14	0.14
Ocean	**Total**	**0,76**	**0.68**	**0,76**	**0.65**
	Low	0,52	0.42	0,57	0.43
	Mid	0,30	0.23	0,18	0.17
	High	0,34	0.33	0,17	0.16

Figure 1: One Orbit.

(ii) ATtenuated Backscattered (ATB) signal, Caliop level 1product, 583 vertical levels
(iii)Lidar Scattering Ratio (SR) over the 40 vertical equidistant levels grid
(iv)GOCCP diagnostics: cloudy, clear, uncertain, fully attenuated (SAT), below the surface level (SE).
(v) Example of one single vertical profile of the scattering ratio for the standard 40 levels grid and the coarse 19 levels grid: vertical bars correspond to the diagnostic thresholds (SR=5, SR=1.2, SR=0.01). The red horizontal lines show the limits of the low-mid-high atmospheric layers.

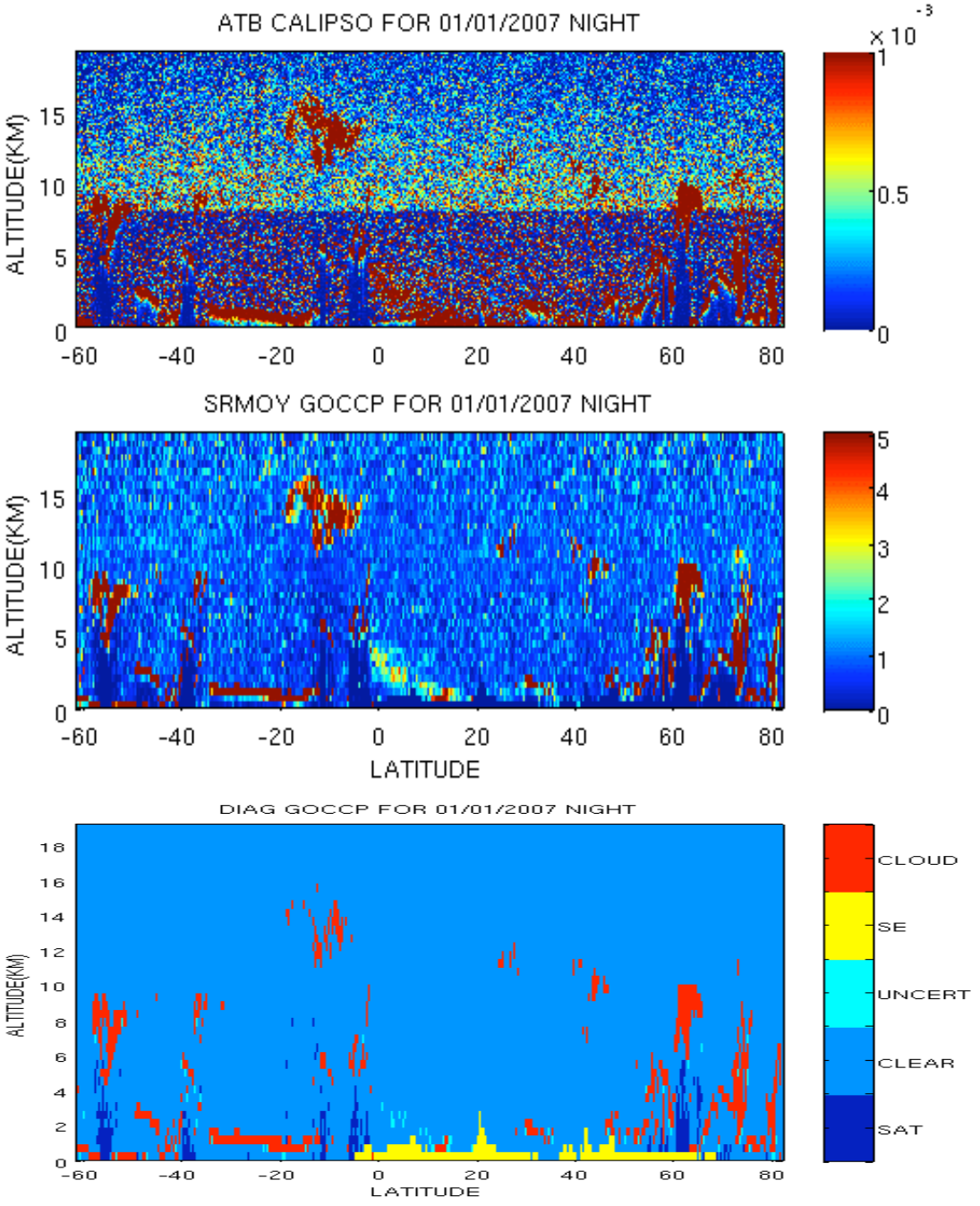

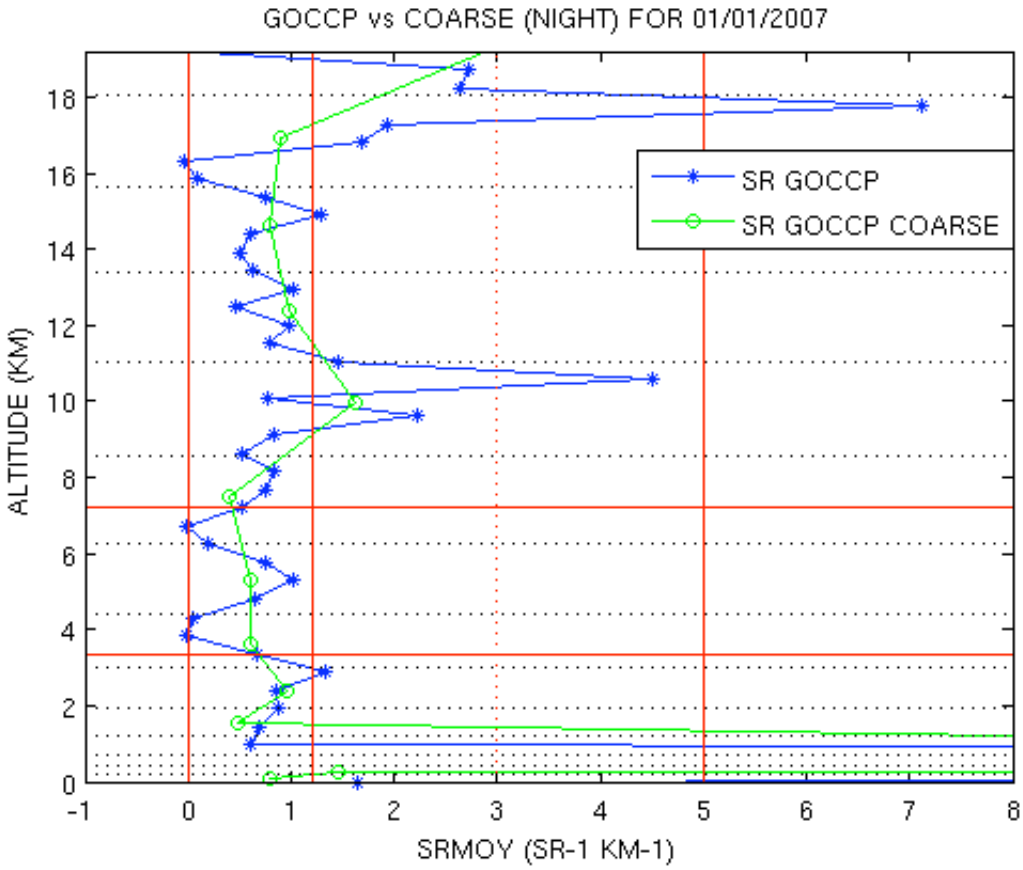
GOCCP vs COARSE (NIGHT) FOR 01/01/2007
SR GOCCP
SR GOCCP COARSE
ALTITUDE (KM)
SRMOY (SR-1 KM-1)
0
2
4
6
8
10
12
14
16
18
-1
0
1
2
3
4
5
6
7
8

Figure 2: Same as 1 for one day time orbit. In c), the white lines correspond to regions where the profiles have been rejected because the noise was too large (see text).

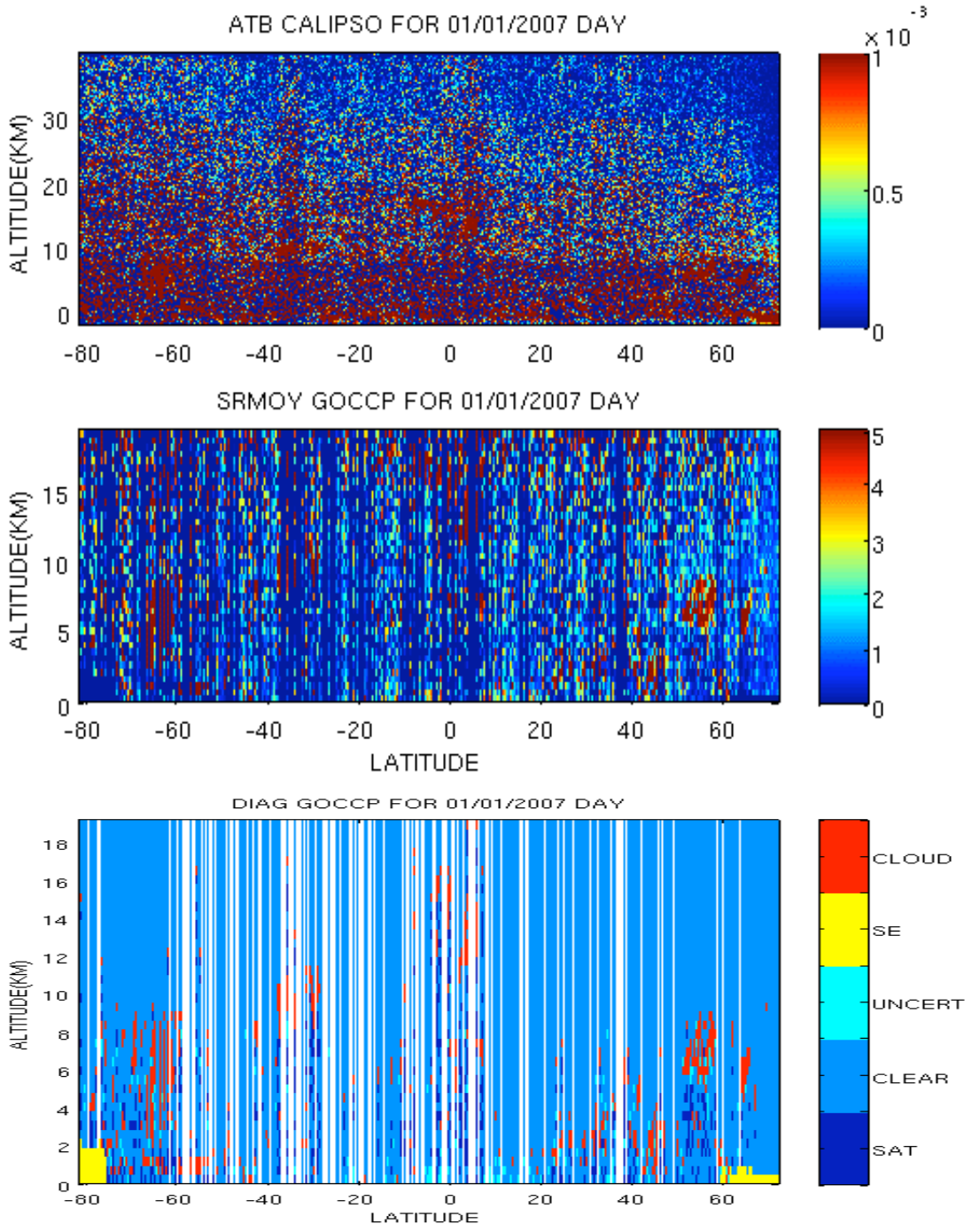

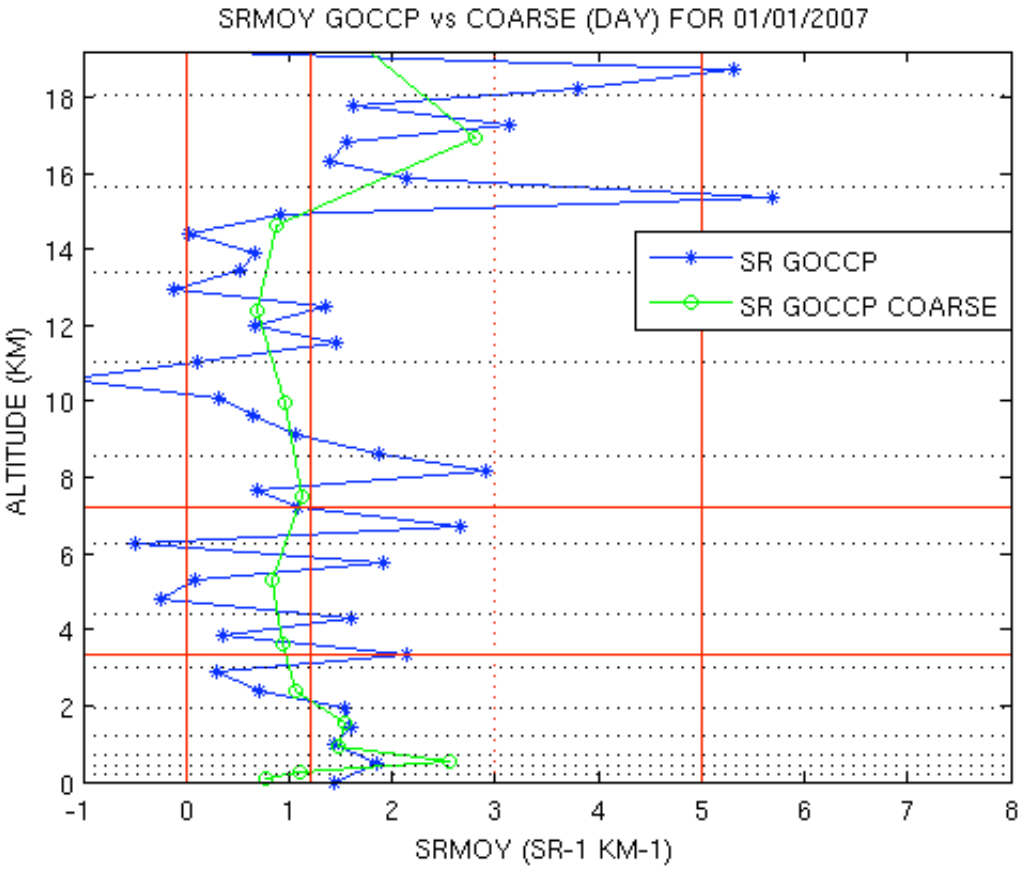
SRMOY GOCCP vs COARSE (DAY) FOR 01/01/2007
ALTITUDE (KM)
SRMOY (SR-1 KM-1)
SR GOCCP
SR GOCCP COARSE
0
2
4
6
8
10
12
14
16
18
-1
0
1
2
3
4
5
6
7
8

Figure 3: GOCCP (a, b) total (c, d) upper-level (e, f) middle-level and (g,h) low-level cloud fraction (averaged over day and night) for JFM (left column) and JJA (right column).

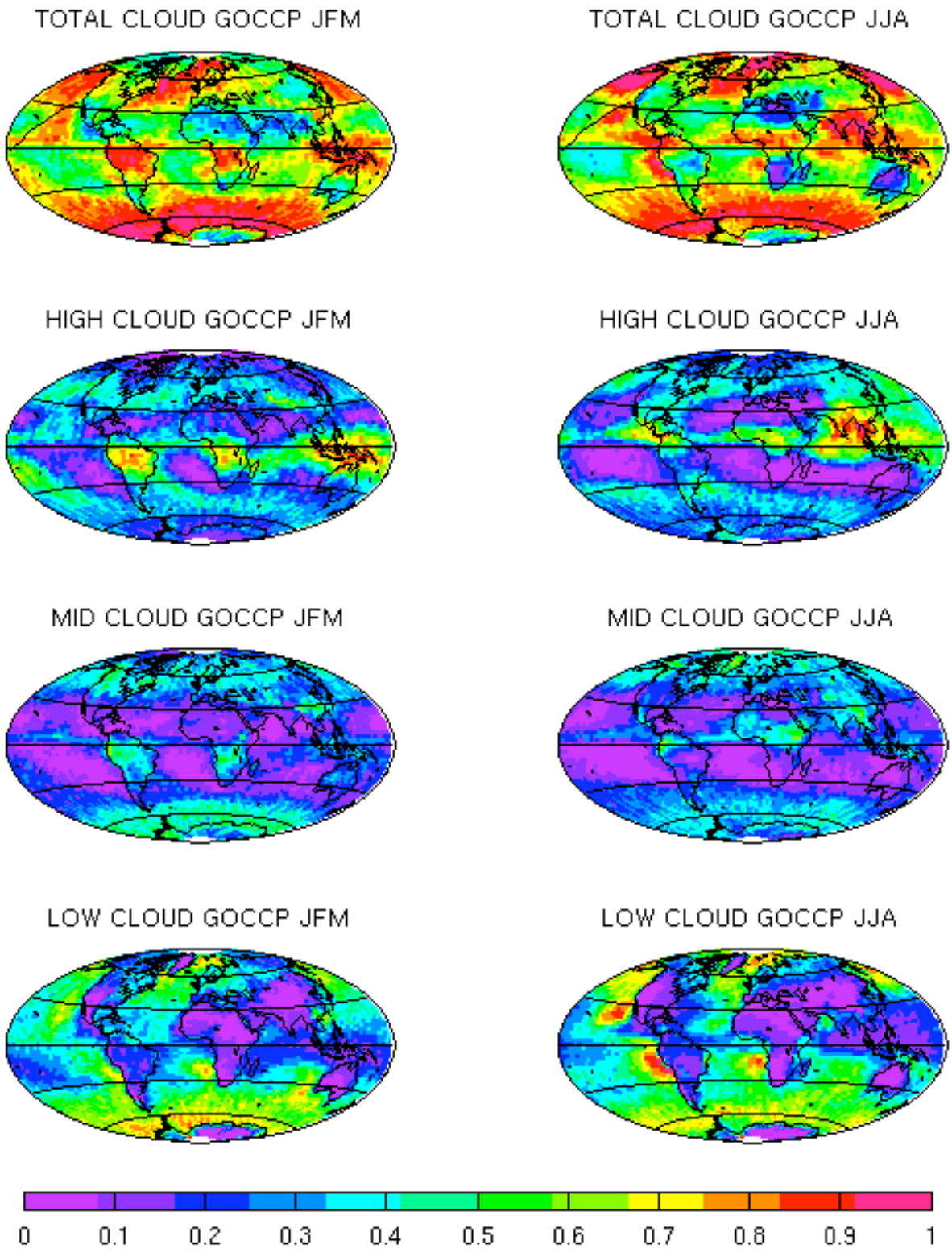

Figure 4: Vertical distributions of the GOCCP cloud fraction for JJA and JFM (GOCCP-SR5)

Zonally-averaged fractions of the longitude-latitude gridboxes flagged as Cloudy ((a) for JJA, (b) for JFM),(c) Clear JJA, (d) Uncertain JJA.

In each longitude-latitude gridbox and each atmospheric layer, the sum of the fractions (a)+(c)+(d) = 1.

The red horizontal lines show the limits of the low-mid-high atmospheric layers used to defined the layered cloud fractions.

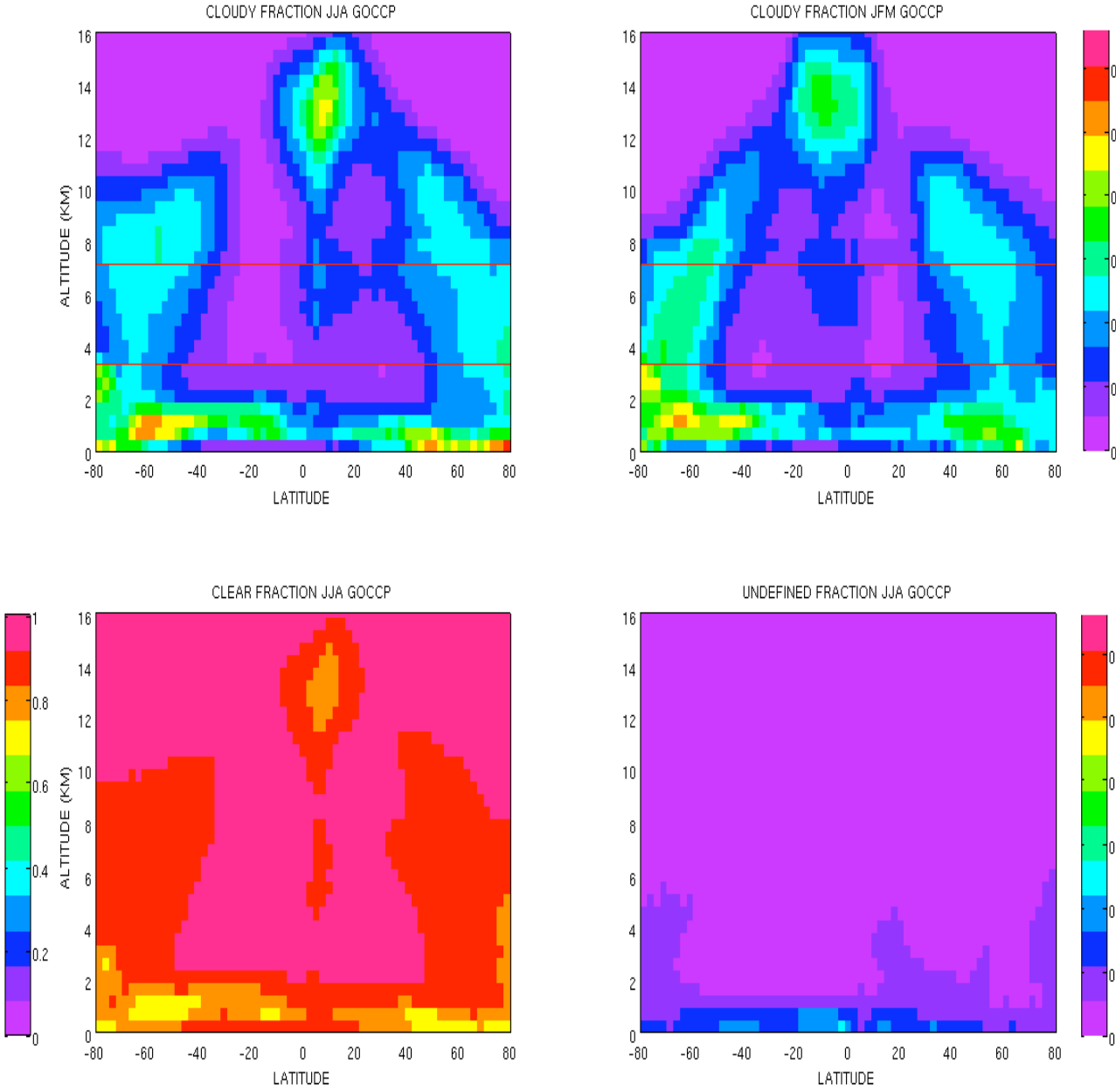

Figure 5: Joint height-SR histogram for JFM (left column) and JJA (right column) derived from GOCCP night-time data for four different regions, from the top to the bottom :

Tropical Western Pacific (5°S-20°N ; 70°-150°E)

California Stratus Region (15-35°N ; 110-140°W)

Hawaian trade cumulus (15-35°N ; 140°W-160°E)

North Pacific (30-60°N ; 160°E-140°W)

On each plot, the vertical axis is the altitude (in km) and the horizontal axis is the SR value.

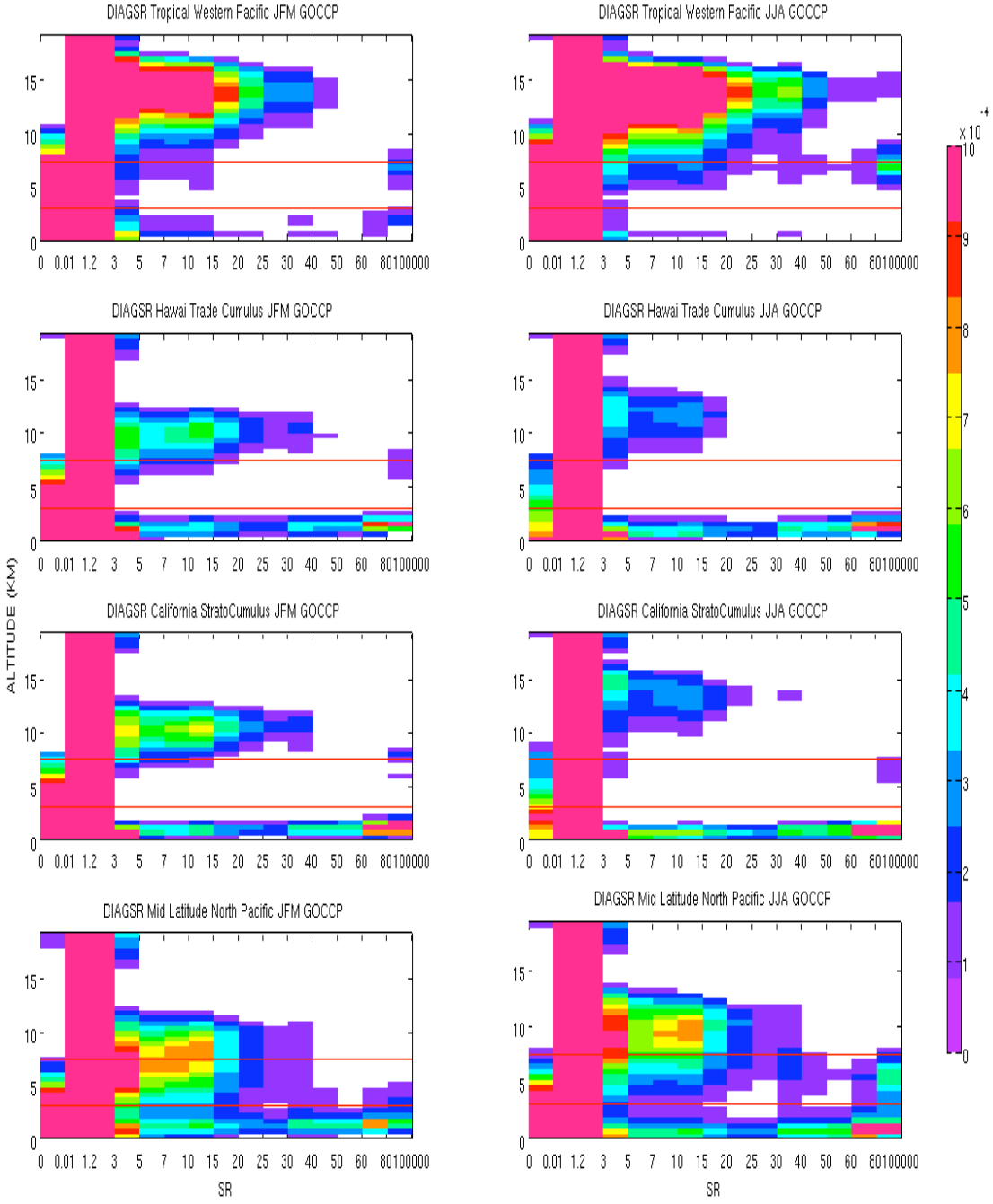

Figure 6: Sensitivity to the vertical grid day/night
Zonal mean (a, e) total (b, f) upper-level (c, g) middle-level and (d) low-level cloud fraction (averaged over day and night) for JFM and JJA. above land (black), above sea (blue), and global (red). The lines without symbols are for the 40 levels grid and the lines with crosses for the coarse grid.

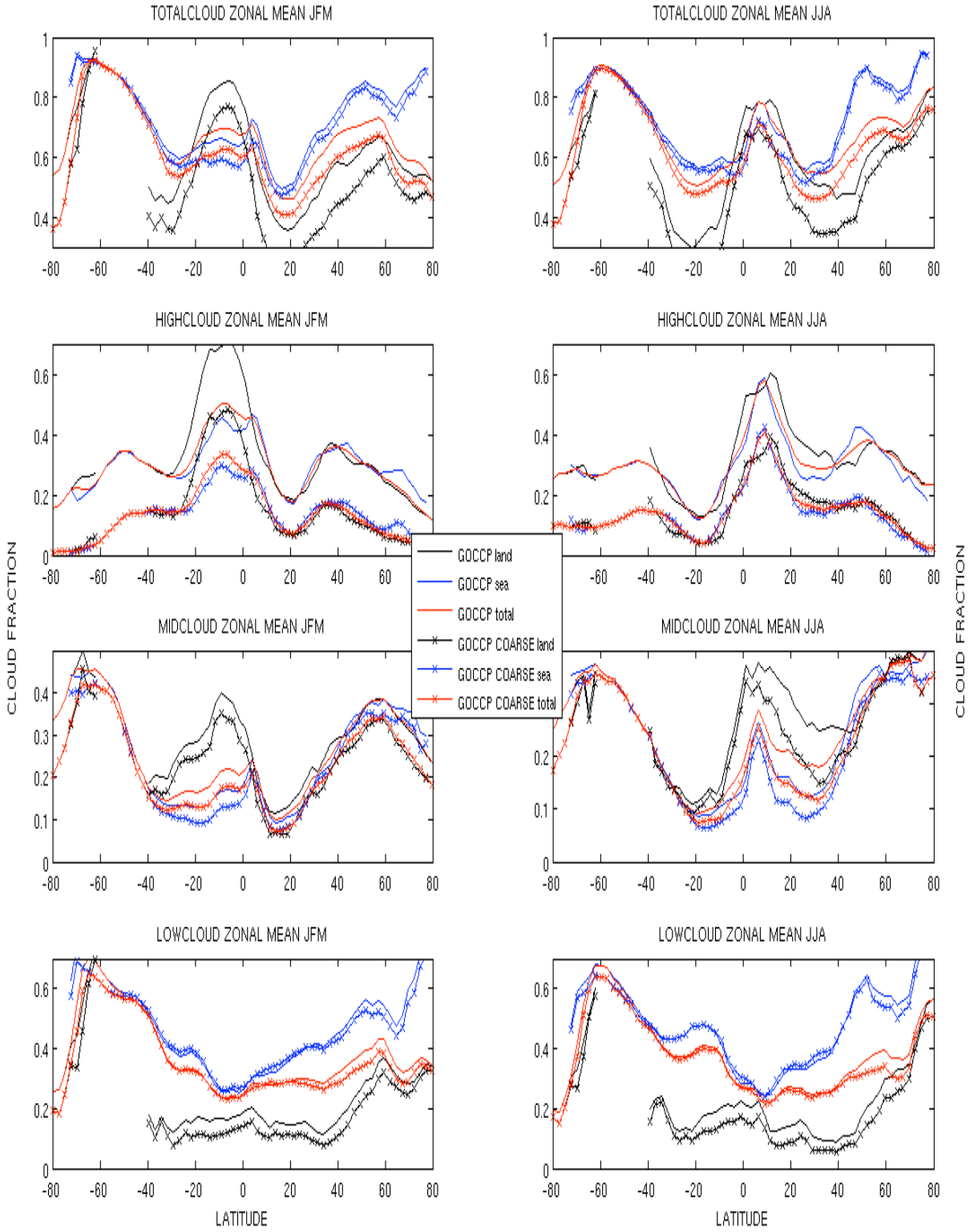

Figure 7: Difference between the cloud fractions diagnosed with a cloud detection threshold SR=3 and SR=5 (JJA, day/night average)

a) Total b) Mid c) Low cloud fraction

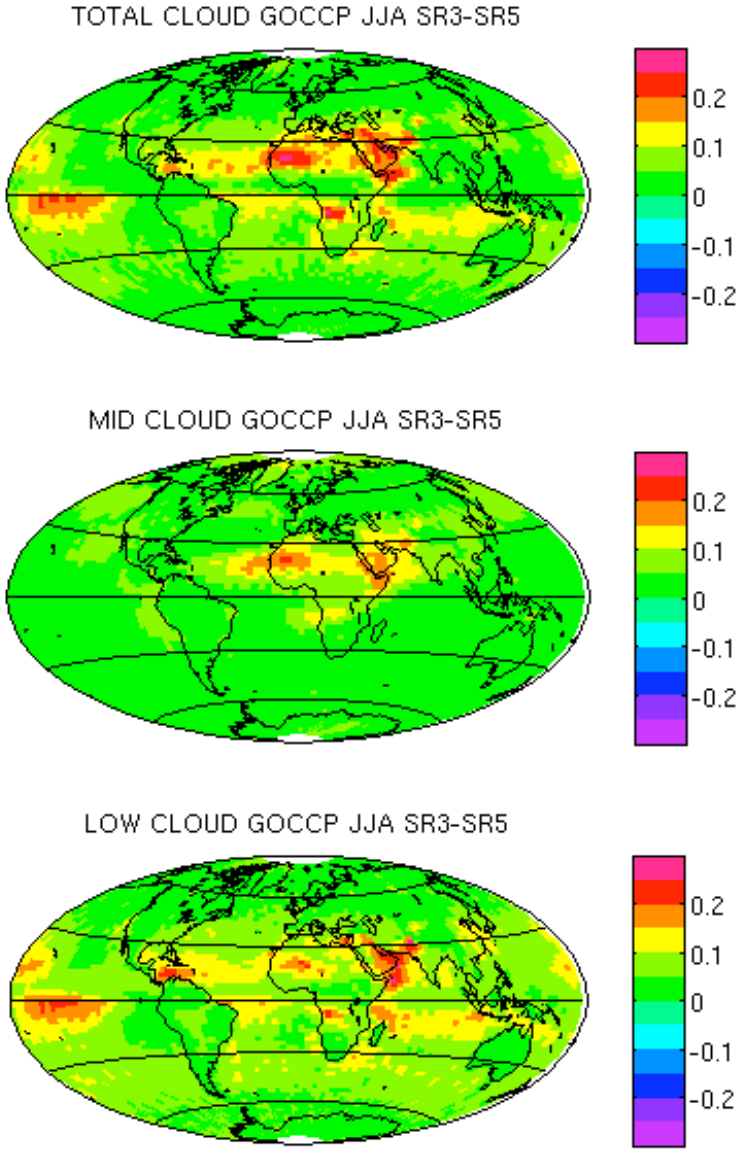

Figure 8 : Cloud cover difference between Day-time and Night-time GOCCP data for JJA

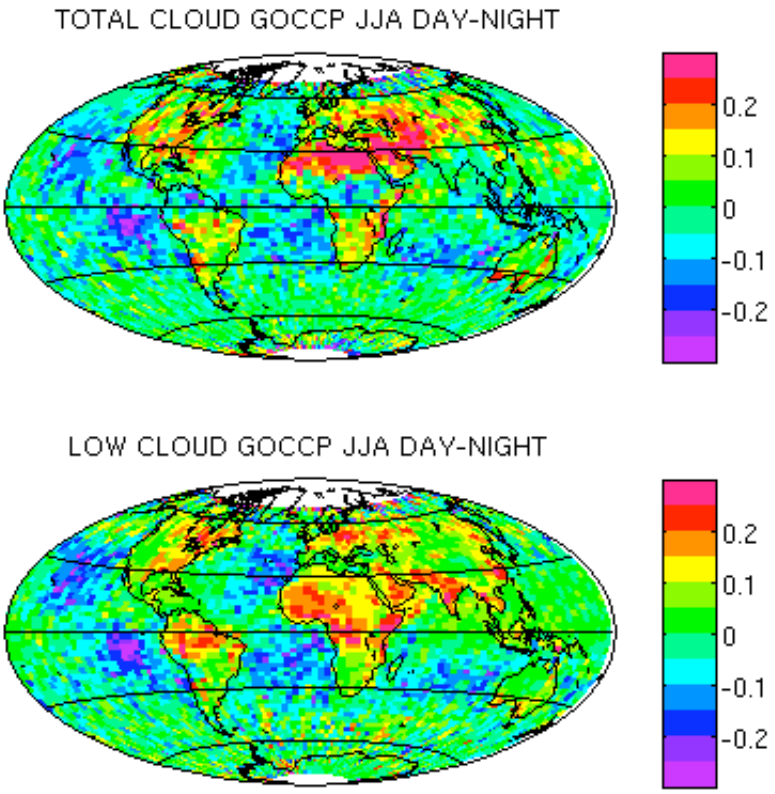

Figure 9: Cloud Fraction along the GCSS Pacific Cross-Section Intercomparison (GPCI) transect (that extends over the Pacific from California to the ITCZ) in JJA

1. Vertical distribution of the Cloud fraction (b) Low, Mid, High and total cloud fractions

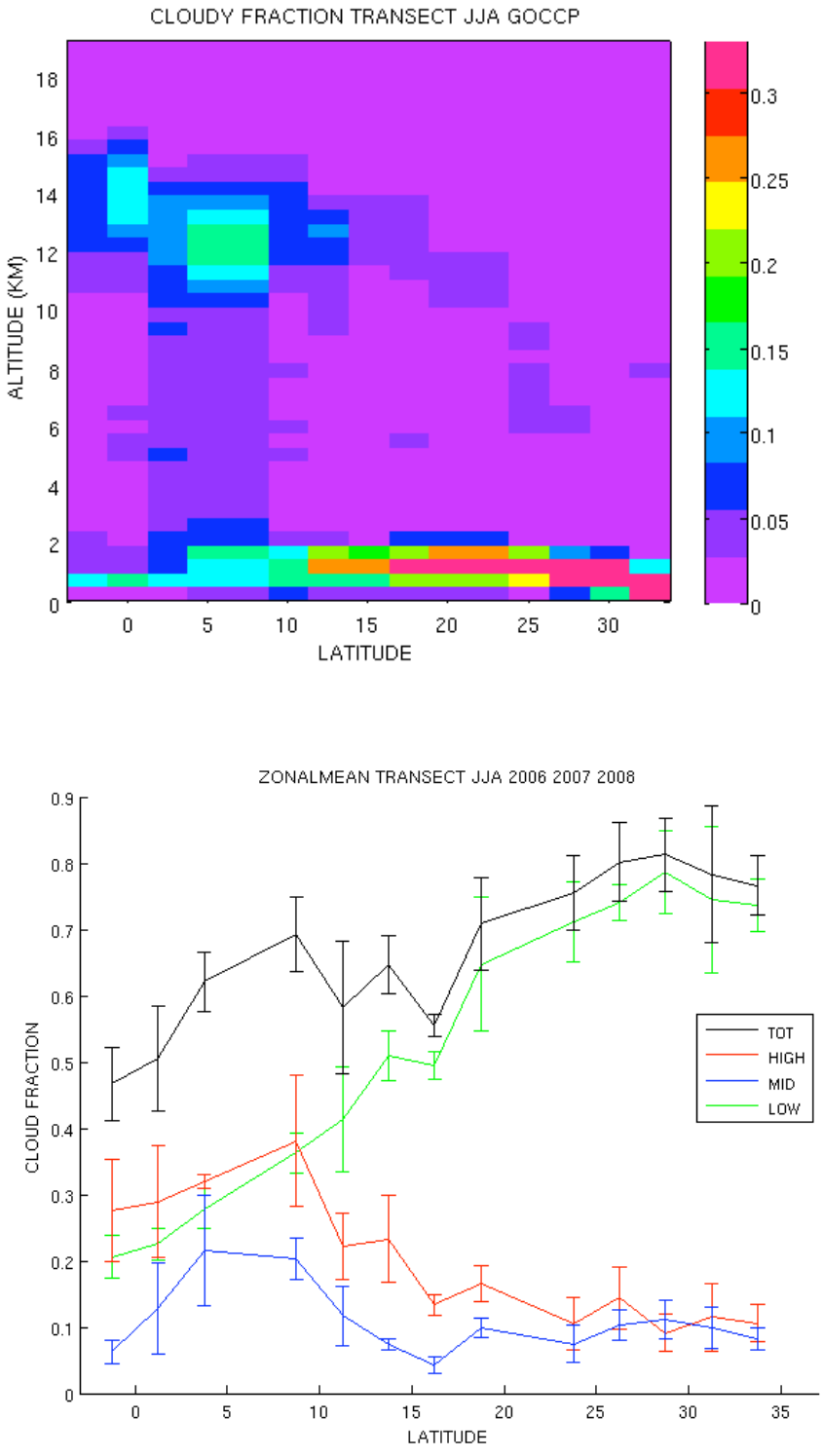

Figure 10: Comparison of GOCCP with others climatologies (annual means).

O= Ocean, L= Land

CALIPSO-GOCCP-SR5 (06-08) , CALIPSO-GOCCP-SR5 (06-08) no overlap (no cloud above), CALIPSO-GOCCP-SR3 (06-08), AIRS-LMD (03-08) , ISCCP (84-04), MODIS-CERES (02-07), TOVS-B (87-95), PARASOL/POLDER (06-08)